

Kinetics of Bacterial Fluorescence Staining with 3,3'-Diethylthiacyanine

Marlon S. Thomas,^{†,‡} Vicente Nuñez,^{†,‡} Srigokul Upadhyayula,^{†,‡,§} Elizabeth R. Zielins,[†]
Duoduo Bao,^{†,‡} Jacob M. Vasquez,^{†,‡,§} Baharak Bahmani,^{†,‡} and Valentine I. Vullev^{*,†,‡,§}[†]Department of Bioengineering, [‡]Center for Bioengineering Research, and [§]Department of Biochemistry,
University of California, Riverside, California 92521

Received July 8, 2009

For more than a century, colorimetric and fluorescence staining have been the foundation of a broad range of key bioanalytical techniques. The dynamics of such staining processes, however, still remains largely unexplored. We investigated the kinetics of fluorescence staining of two Gram-negative and two Gram-positive species with 3,3'-diethylthiacyanine (THIA) iodide. An increase in the THIA fluorescence quantum yield, induced by the bacterial dye uptake, was the principal reason for the observed emission enhancement. The fluorescence quantum yield of THIA depended on the media viscosity and not on the media polarity, which suggested that the microenvironment of the dye molecules taken up by the cells was restrictive. The kinetics of fluorescence staining did not manifest a statistically significant dependence neither on the dye concentration, nor on the cell count. In the presence of surfactant additives, however, the fluorescence-enhancement kinetic patterns manifested species specificity with statistically significant discernibility.

Introduction

This article describes the dynamics of fluorescence enhancement induced in 3,3'-diethylthiacyanine iodide (THIA) upon uptake by bacterial cells (Scheme 1). Although it did not show a statistically significant dependence on the dye concentration and on the bacterial cell count, the kinetics of fluorescence enhancement differed for different bacterial species when they were pretreated with a surfactant additive, TWEEN 40.

Bacterial infectious diseases remain one of the major health hazards worldwide. A quarter of worldwide deaths are a corollary of bacterial infections.^{1–4} Annually, pneumococcal diseases, for example, claim close to a million children's lives worldwide.⁵ In the United States, food-borne bacterial infections cause millions of illnesses, thousands of which are fatal.^{6–8} The expedience of the detection and identification of such pathogens determines how early the diagnosis is made and hence establish the treatment and the outcome of the illness.^{1,9,10}

Because of their simplicity and operational expedience, colorimetric and fluorescence/luminescence staining are the basis of

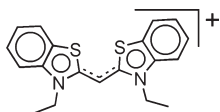
broadly used analytical techniques for biomolecules,^{11–21} bacterial species,^{22–28} eukaryotic cells,^{29–34} and tissue samples.^{35–39} Because of its inherent sensitivity, fluorescence staining is a central component of bioanalytical assays and imaging methodologies.^{40–45}

*Corresponding author. E-mail: vullev@ucr.edu.

- (1) Millar, B. C.; Xu, J.; Moore, J. E. *Curr. Issues Mol. Biol.* **2007**, *9*, 21–40.
- (2) Cossart, P.; Sansonetti, P. J. *Science* **2004**, *304*, 242–248.
- (3) Kumble, K. D. *Mini-Rev. Med. Chem.* **2006**, *6*, 1275–1283.
- (4) Anderson, J. et al. *Basic Research on Bacteria: The Essential Frontier*; American Society for Microbiology and National Institutes of Health, **2007**.
- (5) Scott, J. A. G. *Vaccine* **2007**, *25*, 2398–2405.
- (6) Rose, J. B.; Epstein, P. R.; Lipp, E. K.; Sherman, B. H.; Bernard, S. M.; Patz, J. A. *Environ. Health Perspect.* **2001**, *109*, 211–221.
- (7) Shea, K. M. *Pediatrics* **2000**, *106*, 1505–1510.
- (8) Young, A. L. *Environ. Sci. Pollut. Res. Int.* **2003**, *10*, 82–88.
- (9) Overbye, K. M.; Barrett, J. F. *Drug Discovery Today* **2005**, *10*, 45–52.
- (10) Maloy, S.; Schaechter, M. *Int. Microbiol.* **2006**, *9*, 1–7.
- (11) Deligeorgiev, T. G.; Kaloyanova, S.; Vaquero, J. J. *Recent Pat. Mater. Sci.* **2009**, *2*, 1–26.
- (12) Steinberg, T. H. *Methods Enzymol.* **2009**, *463*, 541–563.
- (13) Cable, M. L.; Kirby, J. P.; Levine, D. J.; Manary, M. J.; Gray, H. B.; Ponce, A. J. *Am. Chem. Soc.* **2009**, *131*, 9562–9570.
- (14) Ghosh, A.; Shrivastav, A.; Jose, D. A.; Mishra, S. K.; Chandrakanth, C. K.; Mishra, S.; Das, A. *Anal. Chem.* **2008**, *80*, 5312–5319.
- (15) Ploeger, L. S.; Dullens, H. F. J.; Huisman, A.; van Diest, P. J. *Biotech. Histology* **2008**, *83*, 63–69.
- (16) Cable, M. L.; Kirby, J. P.; Sorasaene, K.; Gray, H. B.; Ponce, A. J. *Am. Chem. Soc.* **2007**, *129*, 1474–1475.

- (17) Vullev, V. I.; Wan, J.; Heinrich, V.; Landsman, P.; Bower, P. E.; Xia, B.; Millare, B.; Jones, G., II. *J. Am. Chem. Soc.* **2006**, *128*, 16062–16072.
- (18) Miller, I.; Crawford, J.; Gianazza, E. *Proteomics* **2006**, *6*, 5385–5408.
- (19) Jones, G., II; Vullev, V. I. *Photochem. Photobiol. Sci.* **2002**, *1*, 925–933.
- (20) Jones, G., II; Vullev, V. I. *J. Phys. Chem. A* **2002**, *106*, 8213–8222.
- (21) Patton, W. F., Ed.; *Protein Protocols Handbook*, 2nd ed.; Humana Press: Totowa, NJ, 2002; pp 273–286.
- (22) Green, L. H. Diagnostic Medical Microbiology. In *Practical Handbook of Microbiology*, 2nd ed.; Goldman, E., Green, L. H., Eds.; CRC Press: Boca Raton, FL, 2009; pp 117–129.
- (23) Kohlerschmidt, D. J.; Musser, K. A.; Dumas, N. B. In *Practical Handbook of Microbiology*, 2nd ed.; Goldman, E., Green, L. H., Eds.; CRC Press: Boca Raton, FL, 2009; pp 67–79.
- (24) Chapin, K. C.; Lauderdale, T.-L. In *Manual of Clinical Microbiology*, 9th ed.; Murray, P. R.; Baron, E. J.; Tenover, J. C.; Tenover, F. C., Eds.; ASM Press: Washington, DC, 2007; Vol. 1, pp 334–364.
- (25) Nybroe, O.; Brandt, K. K.; Nicolaisen, M. H.; Soerensen, J. In *Modern Soil Microbiology*, 2nd ed.; van Elsas, J. D., Jansson, J. K., Trevors, J. T., Eds.; CRC Press: Boca Raton, FL, 2007; pp 283–316.
- (26) Popescu, A.; Doyle, R. J. *Biotech. Histochem.* **1996**, *71*, 145–151.
- (27) Kaplan, M. L.; Kaplan, L. *J. Bacteriol.* **1933**, *25*, 309–321.
- (28) Veal, D. A.; Deere, D.; Ferrari, B.; Piper, J.; Attfield, P. V. *J. Immunol. Methods* **2000**, *243*, 191–210.
- (29) Gill, M. R.; Garcia-Lara, J.; Foster, S. J.; Smythe, C.; Battaglia, G.; Thomas, J. A. *Nat. Chem.* **2009**, *1*, 662–667.
- (30) Benbow, R. M. *Sci. Prog.* **1992**, *76*, 425–450.
- (31) Kaplan, D. *Cell. Aspects HIV Infect.* **2002**, 351–369.
- (32) Vogt, R. F., Jr.; Schwartz, A.; Marti, G. E.; Whitfield, W. E.; Henderson, L. O. *Methods Mol. Med.* **2001**, *55*, 255–273.
- (33) Crissman, H. A.; Steinkamp, J. A. *Methods Cell Biol.* **2001**, *63*, 131–148.
- (34) Vogt, R. F., Jr.; Whitfield, W. E.; Henderson, L. O.; Hannon, W. H. *Methods (Orlando, Florida)* **2000**, *21*, 289–296.
- (35) Masters, B. R. J. *Biophoton.* **2009**, *2*, 127–139.
- (36) Horny, H.-P.; Sotlar, K.; Valent, P. *Leuk. Res.* **2007**, *31*, 1609–1616.
- (37) Hofecker, J. L.; Moss, T. L.; Becher, M. W. *J. Histotechnol.* **2007**, *30*, 67–78.
- (38) Jeans, A.; Esiri, M. *Pract. Neurol.* **2008**, *8*, 303–310.
- (39) Travlos, G. S. *Toxicol. Pathol.* **2006**, *34*, 548–565.
- (40) McArt, D. G.; McKerr, G.; Howard, C. V.; Saezler, K.; Wasson, G. R. *Biochem. Soc. Trans.* **2009**, *37*, 914–917.
- (41) Kricka, L. J.; Fortina, P. *Clin. Chem.* **2009**, *55*, 670–683.
- (42) Stacey, D. W.; Hitomi, M. *Cytometry, Part A* **2008**, *73A*, 270–278.
- (43) Ljosa, V.; Carpenter, A. E. *Trends Biotechnol.* **2008**, *26*, 527–530.
- (44) Straight, A. F. *Methods Cell Biol.* **2007**, *81*, 93–113.
- (45) Jakobs, S. *Biochim. Biophys. Acta, Mol. Cell Res.* **2006**, *1763*, 561–575.

Scheme 1. Structural Formula of 3,3'-Diethylthiacyanine (THIA)



Ever since the first reports from Carl Friedländer and Hans Christian Joachim Gram, published in 1883 and 1884, respectively,^{46,47} the identification of bacterial species using staining techniques has been based solely on the appearance of the stained cells.^{22,26} Hence, the staining analyses yield Boolean outcomes (i.e., in principle, the reagents either stain or do not stain the analyzed bacteria). As a result, each analysis affords a classification of species into only two groups on the basis of the staining patterns. Morphology analysis, for example, is required for further identification.^{22,23} Similarly, Boolean assays with improved specificity (such as immunofluorescence staining)^{48,49} provide information solely about species that are sought. Thus analytes, which are present in the sample but not targeted by the particular stain, may remain undetected.

For more than a century, bacterial staining has been established as a benchmark for analytical and diagnostic techniques.^{22,26} The dynamics of such staining processes, however, still remains largely unexplored. Recently, we demonstrated that the dynamics of staining has the potential to discriminate between species that would be classified within the same group on the basis of a “traditional” stain analysis.⁵⁰

Herein, we describe our investigation of the interaction of a cyanine dye, THIA, with two Gram-negative bacteria, *Escherichia coli* (*E. coli*) and *Enterobacter aerogenes* (*E. aerogenes*), and two Gram-positive bacteria, *Bacillus subtilis* (*B. subtilis*) and *Bacillus sphaericus* (*B. sphaericus*). When taken up by bacterial cells, THIA manifested an increase in its fluorescence quantum yield. This fluorescence enhancement resulted in a significant contrast, allowing for imaging of the stained cells without the removal of the cyanine dye that remained free in the surrounding solution media (Figure 1). An investigation of the solvent dependence of the photophysical properties of THIA revealed that the media viscosity caused the observed emission enhancement. The observed lack of concentration dependence of the species-specific staining kinetics was a principal feature of the dynamics of bacterial staining with THIA.

Results and Discussion

Interaction between Bacterial Cells and THIA. Similar to other cyanine dyes, THIA (Scheme 1) manifested a pronounced affinity for bacterial cells (Figure 1).^{51–53} When taken up by bacterial cells, THIA exhibited (1) a decrease in the molar extinction coefficient and a change in the shape of the absorption spectrum (Figure 2a); (2) an increase in the emission intensity and about a 10 nm red shift in the emission maximum (Figure 2b); and (3) the appearance of emission bands at wavelengths longer than the spectral maxima (Figure 2b). The relative intensities of the long-wavelength emission bands were sensitive to the conditions of staining. These long-wavelength emission bands

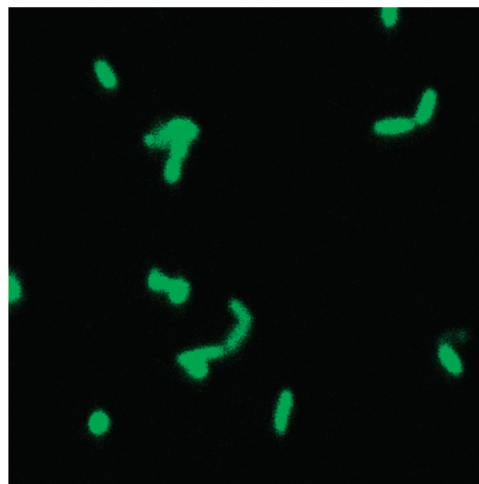


Figure 1. Fluorescent image of *E. coli* in 60 μM THIA solution, recorded with a confocal microscope ($\lambda_{\text{ex}} = 364 \text{ nm}$). The bacterial suspension was deposited on an aminated glass slide with THIA solution (60 μM) and allowed to incubate for 10 min prior to imaging.

were more pronounced in the absence of surfactant and, in general, for cases exhibiting a smaller fluorescence enhancement at 480 nm.

The observed changes in the THIA absorption spectra suggested for ground-state processes that perturbed the electronic structure of the dye upon bacterial uptake. Ground-state isomerization from trans to cis could cause spectral red shifts in THIA upon bacterial uptake.⁵⁴ Although such isomerization could be the reason for the observed red shift in the principal fluorescence band of THIA (from ~ 470 to $\sim 480 \text{ nm}$), the formation of the cis isomer would not be likely to account for the 600 nm emission band (i.e., implied for an $\sim 140 \text{ nm}$ Stokes shift of the cis isomer).

As prevalently observed for pyrene derivatives, for example, ground-state aggregation could be a plausible source of the observed metachromasy.^{55–61} A negatively charged microenvironment combined with hydrophobic interfaces, such as the minor groove in the DNA double strand,^{62–64} binds thiacyanine dyes and propends their aggregation, resulting in pronounced spectral changes.^{65–70} Furthermore, the observed bacterium-induced spectral trends (Figure 2) were in agreement with the reported

(54) Vogt, G.; Krampert, G.; Niklaus, P.; Nuernberger, P.; Gerber, G. *Phys. Rev. Lett.* **2005**, *94*, 068305/068301–068305/068304.

(55) Michaelis, L.; Granick, S. *J. Am. Chem. Soc.* **1945**, *67*, 1212–1219.

(56) Jones, G., II; Vullev, V.; Braswell, E. H.; Zhu, D. *J. Am. Chem. Soc.* **2000**, *122*, 388–389.

(57) Jones, G., II; Vullev, V. I. *Org. Lett.* **2001**, *3*, 2457–2460.

(58) Jones, G., II; Vullev, V. I. *J. Phys. Chem. A* **2001**, *105*, 6402–6406.

(59) Jones, G., II; Vullev, V. I. *Org. Lett.* **2002**, *4*, 4001–4004.

(60) Vullev, V. I.; Jones, G. *Tetrahedron Lett.* **2002**, *43*, 8611–8615.

(61) Vullev, V. I.; Jiang, H.; Jones, G., II. *Top. Fluoresc. Spectrosc.* **2005**, *10*, 211–239.

(62) Patel, M. M.; Anchordoquy, T. J. *Biophys. J.* **2005**, *88*, 2089–2103.

(63) Tolstorukov, M. Y.; Jernigan, R. L.; Zhurkin, V. B. *J. Mol. Biol.* **2004**, *337*, 65–76.

(64) Bostock-Smith, C. E.; Searle, M. S. *Nucleic Acids Res.* **1999**, *27*, 1619–1624.

(65) Benveniste, A. L.; Creeger, Y.; Fisher, G. W.; Ballou, B.; Waggoner, A. S.; Armitage, B. A. *J. Am. Chem. Soc.* **2007**, *129*, 2025–2034.

(66) Tomlinson, A.; Frezza, B.; Kofke, M.; Wang, M.; Armitage, B. A.; Yaron, D. *Chem. Phys.* **2006**, *325*, 36–47.

(67) Hannah, K. C.; Gil, R. R.; Armitage, B. A. *Biochemistry* **2005**, *44*, 15924–15929.

(68) Wang, M.; Silva, G. L.; Armitage, B. A. *J. Am. Chem. Soc.* **2000**, *122*, 9977–9986.

(69) Smith, J. O.; Olson, D. A.; Armitage, B. A. *J. Am. Chem. Soc.* **1999**, *121*, 2686–2695.

(70) Seifert, J. L.; Connor, R. E.; Kushon, S. A.; Wang, M.; Armitage, B. A. *J. Am. Chem. Soc.* **1999**, *121*, 2987–2995.

(46) Friedländer, C. *Fortschr. Med.* **1883**, *1*, 715–733.

(47) Gram, H. C. *Fortschr. Med.* **1884**, *2*, 185–189.

(48) Beutner, E. H.; Holborow, E. J.; Johnson, G. D. *Nature* **1965**, *208*, 353–355.

(49) Levin, P. A. *Methods Microbiol.* **2002**, *31*, 115–132.

(50) Zielins, E.; Thomas, M.; Vullev, V. I. *UCR Undergrad. Res. J.* **2008**, *2*, 75–82.

(51) Miller, J. B.; Koshland, D. E., Jr. *Nature* **1978**, *272*, 83–84.

(52) Anaya, C.; Church, N.; Lewis, J. P. *Proteomics* **2007**, *7*, 215–219.

(53) Roth, B. L.; Poot, M.; Yue, S. T.; Millard, P. J. *Appl. Environ. Microbiol.* **1997**, *63*, 2421–2431.

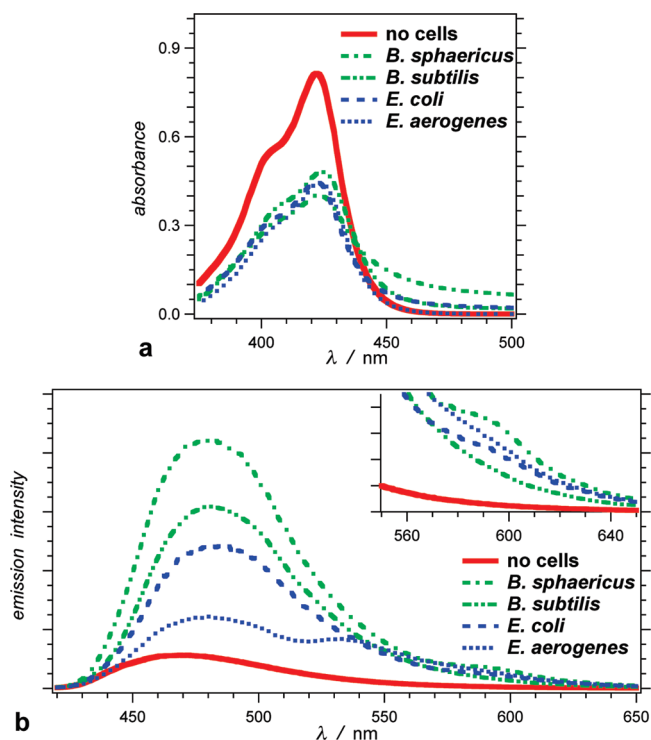


Figure 2. Absorption and fluorescence of THIA ($6 \mu\text{M}$) in the presence and absence of bacterial cells (cell count, $CC = 5 \times 10^7 \text{ cell mL}^{-1}$). All samples were prepared with 2 mM aqueous Tris buffer at pH 8.5 containing 0.5 mM TWEEN 40. The spectra in the presence of bacteria were recorded after 15 min of incubation of the cell suspension with THIA. (a) Absorption spectra. Baseline corrections, using cell suspensions with no dye, were applied. (b) Emission spectra ($\lambda_{\text{ex}} = 420 \text{ nm}$).

metachromic behavior of THIA.^{71,72} Thus, the 600 nm emission peak could be ascribed to a J-like aggregate of THIA taken up by the bacterial cells.⁷¹

We abstain, however, from using the terms H aggregate and J aggregate because they imply a prior knowledge of the relative orientation of the electric transition dipole moments of excitonically coupled dye molecules. Whereas stacked parallel arrangements of the transition dipole moments (i.e., H aggregation) results in blue-shifted spectral features, the head-to-tail arrangement (i.e., J aggregation) results in red-shifted spectral features.^{73–75} These chromophore arrangements, however, are not unique for producing such spectral shifts. Energy shifts in the electronic states of oblique aggregates, for example, can accommodate transitions resulting J- and H-like (red- and blue-shifted) absorption and emission bands.^{73–75}

Because of a lack of structural information on the binding environment for the staining fluorophores, the observed spectral shifts (Figure 2) could not be unambiguously ascribed to J and H structures of THIA aggregates. In fact, each absorption and emission spectrum of the thiocyanine dye in the presence of bacterial cells (Figure 2) represented overlapped spectra from THIA molecules in the environment of different chromotropes (e.g., spectra of monomeric and aggregated THIA bound to bacterial cells overlapped with the spectra of THIA remaining in the

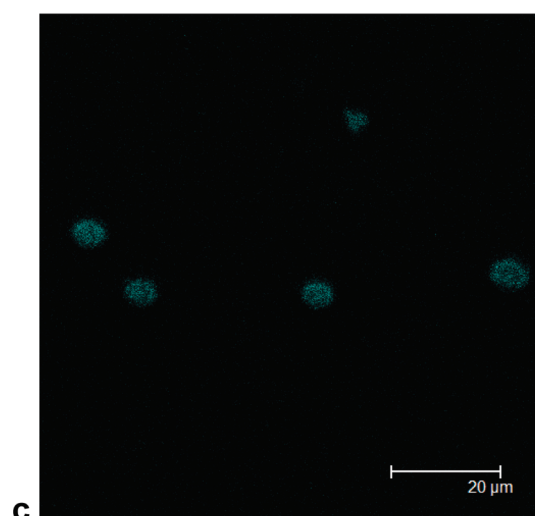
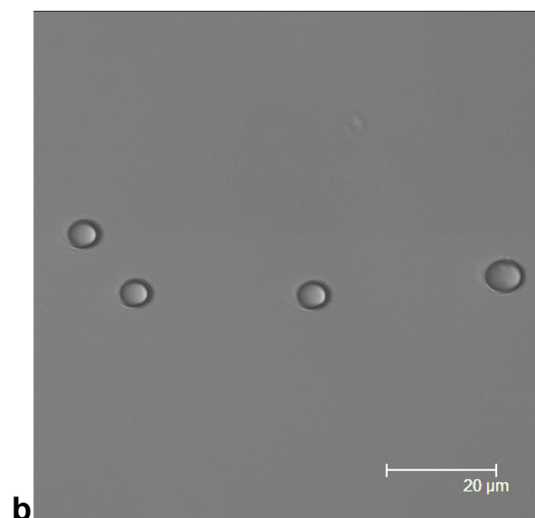
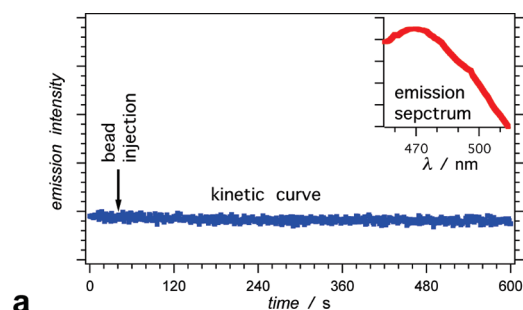


Figure 3. Interaction between THIA and carboxylate-terminated polystyrene beads ($5 \mu\text{m}$ diameter). (a) Kinetic curve ($\lambda_{\text{ex}} = 420 \text{ nm}$, $\lambda_{\text{em}} = 480 \text{ nm}$) and emission spectrum ($\lambda_{\text{ex}} = 420 \text{ nm}$) of THIA ($6 \mu\text{M}$) in the presence of beads ($1.5 \times 10^7 \text{ beads mL}^{-1}$). (b) Phase-contrast image of beads immersed in THIA solution ($600 \mu\text{M}$). (c) Fluorescent image of beads immersed in THIA solution ($600 \mu\text{M}$, $\lambda_{\text{ex}} = 364 \text{ nm}$).

aqueous solution). Furthermore, whereas for most examined species we have observed 600 nm fluorescence bands of different relative intensities, which is in accordance with the previously reported metachromic behavior of THIA,⁷¹ *E. aerogenes* induced a fluorescence band at about 540 nm (Figure 2b).

To examine the phenomena responsible for cell staining and the observed imaging contrast (Figure 1), we investigated the interaction of THIA with negatively charged polystyrene beads. The addition of a bead suspension to the dye solution did not cause emission enhancement (Figure 3a). Fluorescent images, however, revealed

(71) Mandal, A. K.; Pal, M. K. *Chem. Phys.* **2000**, *253*, 115–124.
 (72) Mandal, A. K.; Pal, M. K. *J. Colloid Interface Sci.* **1997**, *192*, 83–93.
 (73) Kasha, M.; Rawls, H. R.; El-Bayoumi, M. A. *Pure Appl. Chem.* **1965**, *11*, 371–392.
 (74) Kasha, M. *Phys. Process. Radiation Biol., Proc. Intern. Symp., Mich. State Univ.* **1964**, pp 17–19, discussion 20–12.
 (75) McRae, E. G.; Kasha, M. *Phys. Process. Radiation Biol., Proc. Intern. Symp., Mich. State Univ.* **1964**, 23–42.

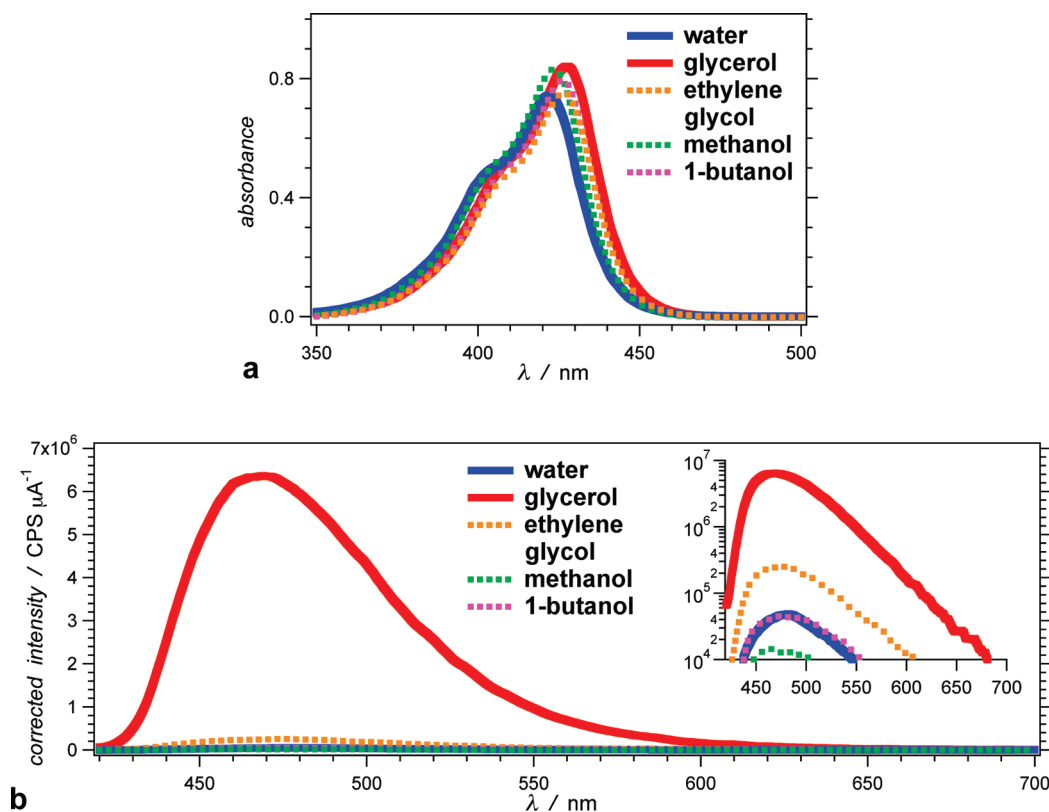


Figure 4. Absorption and emission spectra of THIA ($6 \mu\text{M}$) for water and different alcohols: (a) absorption spectra and (b) emission spectra ($\lambda_{\text{ex}} = 400 \text{ nm}$). The inset represents the same spectra plotted against logarithmic ordinate.

that THIA stains the beads, producing moderate contrast ratios (Figure 3c).

This finding demonstrated that binding of the dye to micrometer-sized objects, such as cells and beads, was a necessary but not sufficient condition for the observed fluorescence enhancement (Figure 2b). The bacteria induced an increase in the emission intensity (Figure 2a), which was accompanied by a decrease in the absorbance of the dye (Figure 2a). Therefore, the dye uptake by the bacteria caused an increase in its fluorescence quantum yield, which along with the increase in the local dye concentration in the cells was a principal reason for the imaging contrast of the stained bacteria (Figure 1).

Solvent Dependence of the Spectral Properties of THIA.

Solvent-dependence measurements of the emission properties of THIA indicated that it is the viscosity, rather than the polarity, of the environment that induced the observed increase in the fluorescence quantum yields (Figure 4).⁷⁶ In fact, in comparison with aqueous media, the fluorescence quantum yield, Φ_f , of THIA increased 1 to 2 orders of magnitude when the dye was placed in solvents more viscous than water (Table 1). For viscous solvents with moderate polarity, glycerol and ethylene glycol, the dye fluorescence quantum yields were $\Phi_f = 0.32$ and $\Phi_f = 0.012$, respectively. In comparison, the Φ_f of THIA did not manifest such a dependence on the polarity of the media (i.e., for a polar medium, water, $\Phi_f = 2.0 \times 10^{-3}$, and for a nonpolar protic solvent, 1-butanol, $\Phi_f = 2.4 \times 10^{-3}$).

In addition, we observed relatively weak solvatochromism, which depended on the excitation wavelength. When excited at 420 nm, for example, THIA exhibited red-shifted fluorescence for relatively low-polarity solvents. Excitation at 410 nm did not produce the same effect. This observation suggested that the

Table 1. Fluorescence Quantum Yield of THIA, Φ_f , for Solvents with Different Dielectric Constants, ϵ , and Different Dynamic Viscosities, η ^a

solvent	$\Phi_f \times 10^3$	ϵ	η/cP
water	2.0	81	0.89
ethylene glycol	12	41	17
glycerol	320	43	930
methanol	0.67	33	0.55
ethanol	1.0	24	1.2
1-butanol	2.4	18	2.5

^aA solution of coumarin 151 in ethanol was used as a standard ($\Phi_f^{\text{(coumarin 151)}} = 0.49$; $\lambda_{\text{ex}} = 400 \text{ nm}$).

underlying effect resulting in bacterium-induced fluorescence red shifts could be a corollary of a decrease in the polarity of the binding microenvironment for THIA. Such wavelength dependence of the fluorescence spectra indicated the heterogeneity of the ground-state population of THIA molecules.

The molecular structure of THIA elucidates the sensitivity of its fluorescence quantum yield to the viscosity of the environment. For cyanine dyes and other molecular rotors with extended π conjugation, the viscosity of the surrounding microenvironment modulates the kinetics of non-radiative decay, which is reflected by changes in the fluorescence quantum yields.^{77–85}

(77) Comotti, A.; Bracco, S.; Valsesia, P.; Beretta, M.; Sozzani, P. *Angew. Chem., Int. Ed.* **2010**, *49*, 1760–1764.

(78) Sutharsan, J.; Lichlyter, D.; Wright, N. E.; Dakanali, M.; Haidekker, M. A.; Theodorakis, E. A. *Tetrahedron* **2010**, *66*, 2582–2588.

(79) Jee, A.-Y.; Kwon, H.; Lee, M. *J. Chem. Phys.* **2009**, *131*, 171104/171101–171104/171104.

(80) Di Paolo, R. E.; Tocho, J. O. *J. Lumin.* **1997**, *72–74*, 481–483.

(81) Grachev, A. V.; Esayan, G. M.; Ponomarev, A. N.; Rubin, L. B.; Yuzhakov, V. I. *Opt. Spektrosk.* **1991**, *70*, 804–807.

(82) Abdel-Mottaleb, M. S. A.; Sherief, A. M. K.; Ismael, L. F. M.; De Schryver, F. C.; Vanderauweraer, M. A. *J. Chem. Soc., Faraday Trans. 2* **1989**, *85*, 1779–1788.

(76) Vasquez, J. M.; Vu, A.; Schultz, J. S.; Vullev, V. I. *Biotechnol. Prog.* **2009**, *25*, 906–914.

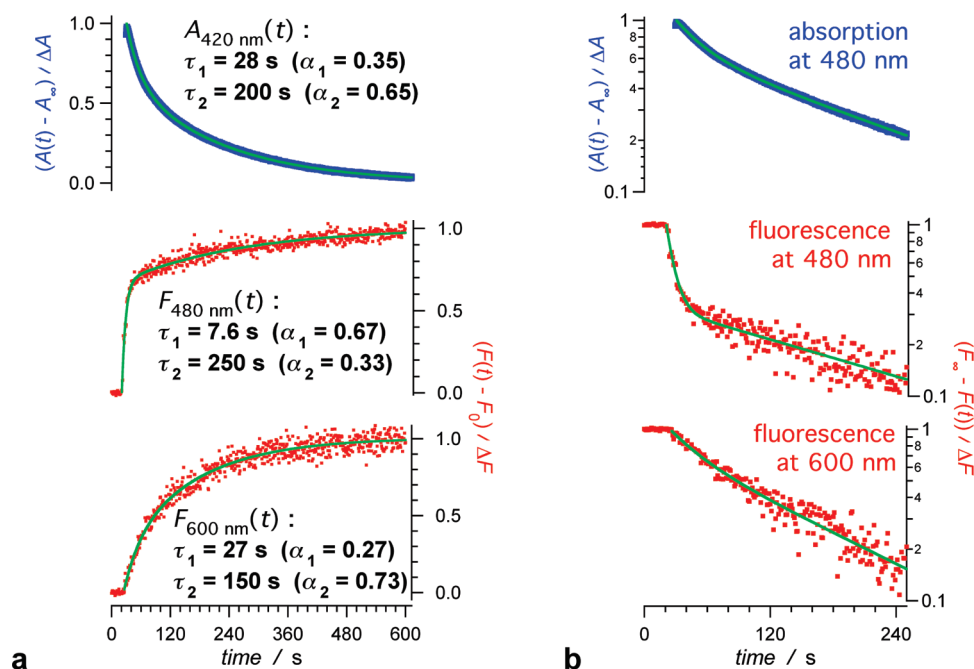


Figure 5. Kinetics of changes induced upon the absorption and emission of THIA ($6 \mu\text{M}$) by *E. coli* ($2 \times 10^7 \text{ cell mL}^{-1}$) for aqueous media buffered with 2 mM Tris buffer at pH 8.5 with no TWEEN added at 37 °C. (a) (Top curve) normalized absorption change monitored at 420 nm ($A_\infty = A_0 - \Delta A$, eq 1b); (middle curve) normalized fluorescence change monitored at 480 nm ($\lambda_{\text{ex}} = 420 \text{ nm}$; eq 1a); and (bottom curve) normalized fluorescence change monitored at 600 nm ($\lambda_{\text{ex}} = 420 \text{ nm}$; eq 1a). (b) The same spectral changes plotted against a logarithmic ordinate. The normalized emission rise features were inverted and represented as decays in order to discern the exponential components with different time constants ($F_\infty = F_0 + \Delta F$, eq 1a).

THIA has a symmetric molecular structure in which extended π conjugation, spanning over the bonds connecting the two ring systems, propends its planar conformation (Scheme 1). Rotational motions around these two bonds, connecting the ring systems, provide pathways for non-radiative decay. An increase in the media viscosity slows down such molecular motions that allow for exploration of the conformational space. As a corollary of the increase in the media viscosity, a decrease in the likelihood of conformational changes leading to non-radiative deactivation results in an increase in the fluorescence quantum yield of the cyanine dye.^{79–87}

The observed viscosity dependence of the emission quantum yield suggested that the fluorescent stain, THIA, migrated from the relatively nonviscous aqueous media into the cell microenvironment with increased viscosity. Upon bacterial uptake, binding of THIA to cell components, which restricted its molecular motion (i.e., providing a microenvironment with a relatively large effective viscosity), resulted in an increase in the dye emission quantum yield causing the observed fluorescence enhancement.

The spectral features of the fluorescence enhancement of THIA induced by bacteria (Figure 2) and by the solvent viscosity (Figure 4) manifested differences that indicated that the cell uptake of the cyanine dye involves more than just binding to a microenvironment that restricts molecular motion. Unlike bacterial cells, viscous solvents did not considerably perturb the absorption spectra of THIA (i.e., glycerol and ethylene glycol caused a slight red shift in the absorption maximum of THIA rather than a

decrease in the molar extinction coefficient (Figure 4a)). Furthermore, neither the red shift of the principal band at 470 nm nor the appearance of new fluorescence bands accompanied the emission enhancement induced by the viscous solvents (Figure 4b).

Dynamics of Bacterium-Induced Spectral Changes. The appearance of the red-shifted emission bands was a feature that set apart the bacterium induced from the solvent-viscosity-induced THIA fluorescence enhancement (Figures 2b and 4b). As we already discussed, such red-shifted fluorescence, along with the observed perturbation of the THIA absorption spectrum upon cell uptake could be ascribed to ground-state aggregation.^{71,72}

To elucidate the relation between the absorption and emission spectral features, we examined the dynamics of their alterations. The time constants, τ_i , representing the kinetics of the bacterium-induced fluorescence enhancement monitored at wavelength λ were extracted from the fit to exponential rise functions,

$$F(t)_{\lambda, t \geq t_0} = \Delta F \left(1 - \sum_{i=1}^n \alpha_i \exp\left(-\frac{t-t_0}{\tau_i}\right) \right) + F_0 \quad (1a)$$

where $F(t)$ is the measured fluorescence intensity over time, t ; F_0 is the initial fluorescence intensity of the dye without bacteria; ΔF is the total increase in the fluorescence intensity; the pre-exponential factors, α_i , sum to unity (i.e., $\sum_{i=1}^n \alpha_i = 1$); and t_0 is the initial time of mixing.

Concurrently, we used a similar exponential decay function to analyze the bacterium-induced changes in the absorption of THIA, $A(t)$, monitored at λ :

$$A(t)_{\lambda, t \geq t_0} = \Delta A \left(-1 + \sum_{i=1}^n \alpha_i \exp\left(-\frac{t-t_0}{\tau_i}\right) \right) + A_0 \quad (1b)$$

We recorded the changes in the absorption of THIA upon addition of *E. coli* (Figure 5). Under identical conditions, we

(83) Kasatani, K.; Sato, H. *Bull. Chem. Soc. Jpn.* **1996**, *69*, 3455–3460.
 (84) Kasatani, K.; Kawasaki, M.; Sato, H. *Chem. Phys.* **1984**, *83*, 461–469.
 (85) Humphry-Baker, R.; Graetzel, M.; Steiger, R. *J. Am. Chem. Soc.* **1980**, *102*, 847–848.
 (86) Sanchez-Galvez, A.; Hunt, P.; Robb, M. A.; Olivucci, M.; Vreven, T.; Schlegel, H. B. *J. Am. Chem. Soc.* **2000**, *122*, 2911–2924.
 (87) Åberg, U.; Åkesson, E.; Alvarez, J. L.; Fedchenia, I.; Sundström, V. *Chem. Phys.* **1994**, *183*, 269–288.

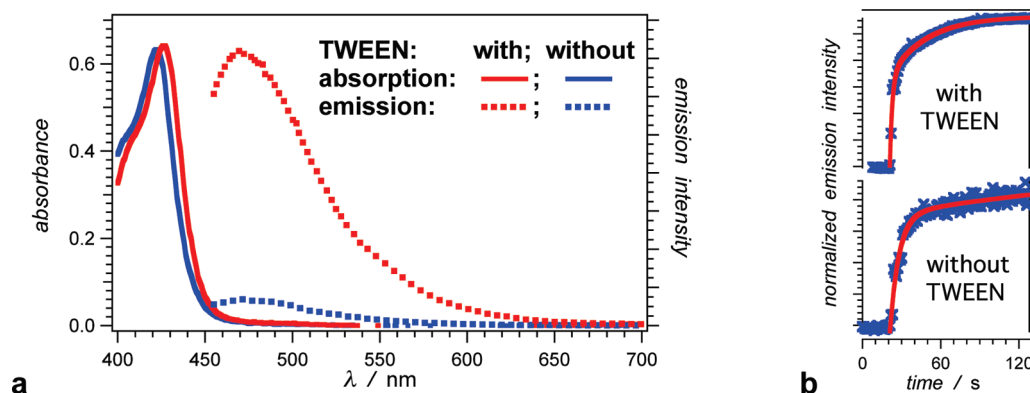


Figure 6. Spectral properties of THIA in the presence and absence of TWEEN. (a) Absorption and emission spectra of THIA ($5 \mu\text{M}$, $\lambda_{\text{ex}} = 420 \text{ nm}$) in the absence and presence of TWEEN 40 ($27 \mu\text{M}$). (b) Kinetics of the THIA emission enhancement ($6 \mu\text{M}$, $\lambda_{\text{ex}} = 420 \text{ nm}$, $\lambda_{\text{em}} = 480 \text{ nm}$) induced by *E. coli* ($5 \times 10^7 \text{ cell mL}^{-1}$) in the absence and presence of TWEEN 40 (0.5 mM). The blue markers, \times , represent the data points; the solid red lines represent the corresponding exponential fits (eq 1a).

recorded the THIA fluorescence enhancement induced by the bacterial cells (Figure 5). The evolution of the absorption and fluorescence kinetic curves exhibited multiexponential patterns. Biexponential functions ($n = 2$, eq 1), however, proved to be the simplest that produced satisfactory data fits (Figure 5). For the absorption decay at 420 nm and for the fluorescence rise at 600 nm , the slow components dominated the kinetics (with time constants ranging between 150 and 250 s). The fast components from the biexponential fits (with time constants of about 30 s) did not conspicuously contribute to the shapes of the kinetic curves and could be visualized solely in plots against logarithmic ordinates (Figure 5b). For the fluorescence enhancement monitored at 480 nm , however, the fast component dominated the kinetics (Figure 5, middle curves). The time constant of the predominant fast components for the 480 nm fluorescence enhancement did not exceed 10 s. It was several-fold faster than the fastest components for the 600 nm emission and the 420 nm absorption kinetics.

The fluorescence enhancement, monitored at 480 nm , exhibits a fast increase within the first 10–20 s of mixing, followed by an additional 25% intensity increase that is considerably slower than the initial jump. The absorption decay at 420 nm and the fluorescence rise at 600 nm , however, exhibited a steady change with kinetic patterns differing from the kinetic pattern observed for the 480 nm fluorescence enhancement (Figure 5). The bacterium-induced perturbation of the absorption spectra and the growth of the long-wavelength emission bands hence appeared to be related. Similar kinetics indicated that they could be a corollary of the same underlying process, reasonably ascribed to THIA aggregation.^{71,72} The minor slow component of the 480 nm fluorescence enhancement could plausibly be ascribed to a similar concurrent aggregation of THIA exhibiting H-like-aggregate emission.⁷¹

The initial fast jump in the fluorescence intensity, monitored at 480 nm , represented the principal emission enhancement induced by the bacterium uptake. The time constant, representing the initial 480 nm fluorescence-intensity increase, was more than 4 times shorter than the shortest time constants for the absorption decay (Figure 5). Therefore, the fast 480 nm fluorescence enhancement did not result from the same processes that caused the perturbation of the absorption spectra (i.e., the principal component of the 480 nm emission enhancement was not caused by dye aggregation). In accordance with the viscosity-dependence quantum-yield findings, we ascribed the fast increase in the THIA fluorescence intensity at $\sim 480 \text{ nm}$ to initial binding of the dye to a cellular chromotropic

microenvironment, which restricted the molecular motion (i.e., the chromotropes provide a fluorogenic microenvironment for THIA).

Effects of TWEEN on the Behavior of THIA. Additives such as mild surfactants modulated the spectral and kinetic features of the bacterium-induced emission enhancement. TWEEN is a mild oligoethylene glycol amphiphath that is regularly employed to prevent cell and protein adhesion without compromising their viability and integrity. In the presence of TWEEN, THIA exhibited spectral changes similar to the changes that we observed for THIA induced by viscous solvents (Figures 4 and 6a) (i.e., the addition of TWEEN 40 to THIA solution caused (1) a slight red shift in the absorption maximum without many other spectral perturbations and (2) an increase in the fluorescence intensity without shifts of the 470 nm maximum (Figure 6a)). The TWEEN 40 surfactant also suppressed the appearance of the long-wavelength emission bands of THIA in the presence of bacteria (Figure 6b).

Furthermore, TWEEN increased the rates of fluorescence enhancement monitored at 480 nm . In the presence of TWEEN, we also observed a fast followed by a slow intensity increase (Figures 6b and 7a). In the presence of TWEEN 40, however, the slow intensity increase was a principal component of the 480 nm kinetics. Monoexponential fits, limited to the time spans of the intensity increase that followed the few-second initial jump of the 480 nm fluorescence, yielded time constants similar to the time constant representing the slow components from the biexponential analyses (Figure 7a). *B. subtilis* in the presence of TWEEN, however, induced an emission enhancement that exhibited solely monoexponential behavior (Figure 7b) (i.e., a fast fluorescence intensity increase (in less than 10 s), which was not followed by a slow kinetic component).

Kinetics of Fluorescence Enhancement for Different Species. For samples containing 0.5 mM TWEEN 40, we examined the kinetics of the fluorescence enhancement for dye concentration C_{THIA} , and cell count CC spreading over 2 orders of magnitude (i.e., THIA concentrations of $C_{\text{THIA}} = 0.6, 6, \text{ and } 60 \mu\text{M}$ and cell counts of $CC = 5 \times 10^6, 5 \times 10^7, \text{ and } 5 \times 10^8 \text{ cell mL}^{-1}$). We focused on the 480 nm steady emission enhancement kinetics that followed the initial intensity jump upon mixing (Figure 7a). For each of the examined species, the obtained values of the emission-enhancement time constants did not significantly vary over the investigated dye concentration and cell-count ranges (Table 2). The time constant, however, differed for the four investigated species (Table 2). The values of the time constants for *E. coli* were clustered around 30 s: for *E. aerogenes*, around

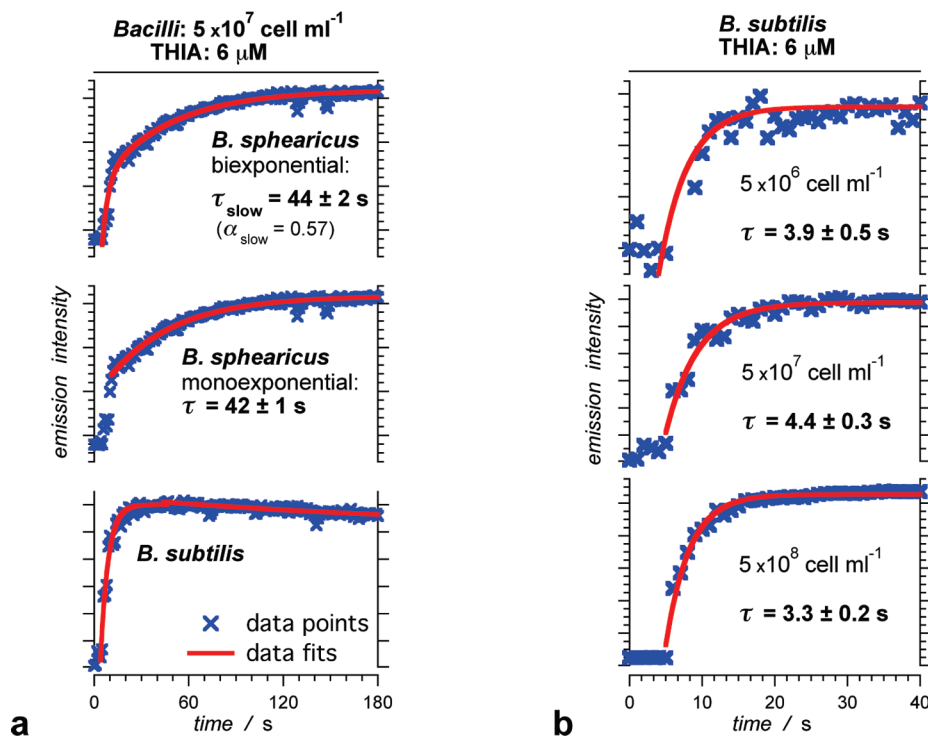


Figure 7. Fluorescence-enhancement kinetic curves ($\lambda_{\text{ex}} = 420$ nm, $\lambda_{\text{em}} = 480$ nm, 37°C) for *bacilli* samples injected into $6 \mu\text{M}$ THIA solution (at $t_0 \approx 5$ s, eq 1a). All samples were prepared with 2 mM aqueous Tris buffer at pH 8.5 containing 0.5 mM TWEEN 40. (a) Kinetic curve for 5×10^7 cell mL^{-1} *B. sphearicus* (top and middle curves) and *B. subtilis* (bottom curve). (The fast rise prior to the slow intensity increase, asymptotically approaching the maximum fluorescence intensity, was characteristic of pretreatment with TWEEN surfactant for *B. sphearicus*, *E. coli*, and *E. aerogenes*.) For *B. sphearicus*, the monoexponential analysis yielded a time constant almost identical to the time constant corresponding to the slow component of the biexponential rise. (b) Kinetic curves for different cell counts of *B. subtilis* with the corresponding monoexponential fits ($n = 1$, eq 1). The error values represent the standard deviations yielded by the least-squares algorithms for each data fit.

20 s; for *B. subtilis*, around 3 s; and for *B. sphearicus*, around 50 s (Table 2).

Analysis of variance (ANOVA) allowed us to examine the observed trends in the concentration and species dependence of the emission-enhancement time constants. For each species, we employed two-factor ANOVA tests. The two null hypotheses for each of the tests stated that the time constants for the different cell counts and for the different dye concentrations were identical. The obtained p values for the cells and for the dye were large enough to prevent the reasonable rejection of either of the null hypotheses (Table 2).

To examine the discernibility between the time constants for the different species, we employed one-factor ANOVA tests. Each test compared the emission-enhancement kinetics for two different species with the null hypothesis (H_0) that the time constants for these two bacteria are identical. Neither of the six p values for the possible combination between the four investigated species exceeded 10^{-5} , corresponding to minute probabilities (i.e., $< 0.001\%$) for experiments to yield the values of τ , which we observed, if H_0 was true (Table 3). Therefore, we could confidently reject the null hypothesis for all comparisons between the bacterial species (i.e., the kinetics of staining with THIA in the presence of TWEEN 40 was species-specific).

One of the most important implications of these findings (i.e., important for assay developments) was that the staining kinetic curves for two closely related species, *B. subtilis* and *B. sphearicus*, were different (Figure 7). Furthermore, whereas *B. sphearicus* exhibited the slowest kinetic features, *B. subtilis* showed the fastest staining kinetics among the examined species (Table 2).

This discernibility between the staining kinetics for the different investigated bacterial species, however, was induced by surfactant additive TWEEN 40. In the absence of a surfactant, the sub-10-s initial rise dominated the emission-enhancement kinetics at 480 nm (Figures 5 and 6c). This kinetics analysis, obtained in the absence of TWEEN 40, revealed that for each species the time constants were not statistically dependent on the dye concentration and on the cell count. The values of the obtained time constants for the different bacteria, however, were not sufficiently segregated from one another to serve as a handle for species-specific kinetics (Supporting Information). Therefore, the lack of a surfactant additive did not cause the dependence of the staining kinetics on the dye concentration and on the cell count. The lack of TWEEN 40, however, compromised the kinetics-based discernibility between species.

The species-specific concentration-independent trends that we observed for the emission enhancement time constants (Table 1) applied to samples pretreated with TWEEN 40. We observed similar trends when only the cells were pretreated with TWEEN 40 and added to THIA solution without any surfactant.⁵⁰ Even under such different experimental conditions, we still observed concentration-independent emission-enhancement time constants. For *B. sphearicus*, these time constants were larger than the time constants for *E. coli*, which were larger than the time constants for *B. subtilis*.⁵⁰ Our findings demonstrated that TWEEN 40 considerably modulates the dynamics of uptake of a cationic dye by bacterial cells to provide discernible kinetics for species as similar as the two investigated *bacilli* (Table 2).

Gram-positive species *B. subtilis* and *B. sphearicus* have cell walls that are significantly thicker than the cell walls of the

Table 2. Time Constants, τ/s^a , for the Enhancement of the Fluorescence of THIA Induced by Four Vegetative Bacteria for Different Dye Concentrations, C_{THIA} , and Cell Counts, CC , in the Presence of TWEEN Surfactant^b

$C_{\text{THIA}}/\mu\text{M}$	Gram-negative, $CC/\text{cell mL}^{-1}$			Gram-positive, $CC/\text{cell mL}^{-1}$		
	5×10^6	5×10^7	5×10^8	5×10^6	5×10^7	5×10^8
	<i>E. coli</i> ^c			<i>B. subtilis</i> ^d		
0.6	34 ± 4	33 ± 6	22 ± 6	3.1 ± 1.7	2.2 ± 0.8	3.8 ± 1.4
6	27 ± 2	27 ± 6	29 ± 4	3.9 ± 1.0	3.9 ± 1.6	2.8 ± 1.1
60	31 ± 6	36 ± 5	26 ± 1	5.1 ± 1.1	2.6 ± 0.4	2.9 ± 0.3
	$p_{\text{cell}} = 0.07^e; p_{\text{cell}}^{(\text{NR})} = 0.30^f$ $p_{\text{dye}} = 0.08^e; p_{\text{dye}}^{(\text{NR})} = 0.67^f$			$p_{\text{cell}} = 0.03^e; p_{\text{cell}}^{(\text{NR})} = 0.40^f$ $p_{\text{dye}} = 0.45^e; p_{\text{dye}}^{(\text{NR})} = 0.77^f$		
	<i>E. aerogenes</i> ^c			<i>B. sphaericus</i> ^c		
0.6	21 ± 7	19 ± 5	20 ± 10	52 ± 9	59 ± 6	58 ± 7
6	16 ± 3	17 ± 2	22 ± 3	28 ± 13	52 ± 8	38 ± 12
60	20 ± 3	17 ± 4	20 ± 6	54 ± 7	52 ± 8	51 ± 3
	$p_{\text{cell}} = 0.30^e; p_{\text{cell}}^{(\text{NR})} = 0.30^f$ $p_{\text{dye}} = 0.53^e; p_{\text{dye}}^{(\text{NR})} = 0.50^f$			$p_{\text{cell}} = 0.01^e; p_{\text{cell}}^{(\text{NR})} = 0.35^f$ $p_{\text{dye}} = 0.08^e; p_{\text{dye}}^{(\text{NR})} = 0.10^f$		

^a In bold. ^b Aqueous Tris buffer (2 mM, pH 8.5) with 0.5 mM TWEEN 40; 37 °C; and $\lambda_{\text{ex}} = 420$ nm, $\lambda_{\text{em}} = 480$ nm. The bacterial samples were from cultures in their exponential growth phase. ^c The time constants represent the slower components from biexponential fits (Figure 2a). ^d The time constants were obtained from monoexponential fits. ^e The p values were obtained from two-factor ANOVA analysis of the time constants for the same species with THIA considering all measurement repeats. ^f The nonrepeated p values, $p^{(\text{NR})}$, were obtained from two-factor ANOVA considering solely the average values for each concentration/cell density data point.

Table 3. Results from One-Factor ANOVA Analysis Comparing the Time Constants Obtained for the Four Investigated Species (Table 2)^a

	<i>E. coli</i>	<i>E. aerogenes</i>	<i>B. subtilis</i>
<i>E. aerogenes</i>	$p = 5.1 \times 10^{-12}$ ($F = 79$) ^b $p^{(\text{NR})} = 8.7 \times 10^{-6}$ ($F = 41$) ^c		
<i>B. subtilis</i>	$p < 10^{-16}$ ($F = 730$) ^b $p^{(\text{NR})} = 7.8 \times 10^{-12}$ ($F = 300$) ^c	$p < 10^{-16}$ ($F = 510$) ^b $p^{(\text{NR})} = 1.4 \times 10^{-13}$ ($F = 510$) ^c	
<i>B. sphaericus</i>	$p = 1.7 \times 10^{-10}$ ($F = 63$) ^b $p^{(\text{NR})} = 5.6 \times 10^{-5}$ ($F = 29$) ^c	$p < 10^{-16}$ ($F = 160$) ^b $p^{(\text{NR})} = 1.5 \times 10^{-7}$ ($F = 78$) ^c	$p < 10^{-16}$ ($F = 390$) ^b $p^{(\text{NR})} = 2.8 \times 10^{-10}$ ($F = 190$) ^c

^a For the comparison of the species from each column with the species from each row, the p values were estimated from the F ratios (shown in parentheses), obtained from one-factor ANOVA analysis. ^b For the p values comparing each set of two species, the time constants for all measured repeats, for all THIA concentrations, and for all cell counts were considered. ^c For the nonrepeated p values, $p^{(\text{NR})}$, comparing each set of two species, solely the average time constants for all THIA concentrations and for all cell counts were considered.

Gram-negative species. (The Gram-negative cell walls contain a lipopolysaccharide-coated outer membrane enclosing the peptidoglycan-filled periplasmic space). The Gram-positive cell walls, however, contain only one membrane (i.e., the plasma membrane), and the periplasmic space is coated with a thick peptidoglycan layer. The kinetic patterns for the two TWEEN-pretreated Gram-positive cells manifested the most drastic difference (Figure 4a, Tables 2 and 3). Therefore, the generic chemical composition and the thickness of the cell walls cannot account for the observed kinetic differences. The TWEEN inhibition of the staining rates, observed for *B. sphaericus* but not for *B. subtilis*, suggested that either (1) *B. subtilis* provided more binding sites for THIA, the access to which could not be visibly restricted by the surfactant or (2) *B. sphaericus* had a stronger affinity for TWEEN 40, increasing its inhibiting potency against the uptake of staining dye.

Diffusion-Driven Dye Uptake. The monoexponential and biexponential data fits allowed for quantitative analysis of the emission-enhancement kinetics. Such monoexponential and biexponential treatments, however, were not informative about the lack of a statistically significant dependence of the kinetics on the dye concentration and on the cell count.

Following reports that, upon staining, the taken up cyanine dyes collect in the bacterial cell walls,^{52,53} we modeled the dynamics of fluorescence enhancement as a diffusion-driven migration of the dye from the aqueous environment into a thin

sheet of permeable media (Scheme 2)⁸⁸

$$M(t)_{t \geq t_0} = \frac{m(t)}{m(\infty)} = 1 - \sum_{n=1}^{\infty} \frac{2\alpha(1+\alpha)}{1+\alpha+\alpha^2q_n^2} \exp\left(-\frac{Dq_n^2(t-t_0)}{L^2}\right) \quad (2)$$

$$M(t)_{t < t_0} = 0$$

where the cell wall was modeled as a sheet of media with thickness L ; D , thus, is the THIA diffusion coefficient in the cell-wall media; $m(t)$ is the total mass of THIA in the cell wall at time t ; q_n represents the n th nonzero positive root of $\tan(q_n) = -\alpha q_n$; and α represents the THIA distribution (i.e., $\alpha = A/KL$). In the latter, K is the partition coefficient of THIA between the cell wall and the aqueous medium and A is the characteristic length of the bulk solution that can be expressed in terms of cell count, CC , cell volume, V_C , unit volume, V_1 , and surface area of a cell, S_C (i.e., $A = V_1/(CC \times S_C) - V_C/S_C$).

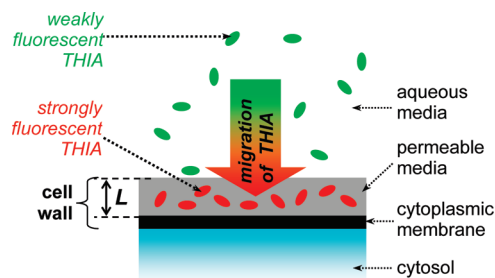
The time-dependent normalized amount of dye taken up, $M(t)$, was indicative of the emission-enhancement kinetics

$$F(t) \propto \frac{M(t)}{\alpha+1} \Phi_C + \frac{\alpha+1-M(t)}{\alpha+1} \Phi_W \quad (3)$$

where Φ_C and Φ_W are the fluorescence quantum yields of the dye in the cells and in the aqueous medium, respectively. Equation 3

(88) Crank, J. Diffusion in a Plane Sheet. In *The Mathematics of Diffusion*, 2nd ed.; Clarendon Press: Oxford, U.K., 1975; pp 44–68.

Scheme 2. Fluorescence Enhancement Due to the Migration of THIA from the Aqueous Surroundings into the Fluorogenic Cell-Wall Medium^a



^aThe cell wall is modeled as a sheet of permeable medium over a membrane, which is not permeable to the dye. The thickness of the permeable sheet is L , and the diffusion coefficient of the dye in the sheet is D . For Gram-positive species, the permeability is a simplified representation of the peptidoglycan coating of the periplasmic side of the cytoplasmic membrane. For Gram-negative species, this representation of the cell wall is indeed a further oversimplification approximating the periplasmic space with the peptidoglycan layer, the outer membrane, and the lipopolysaccharide layer as a homogeneous permeable sheet layer. Nevertheless, this simplistic model allows us to elucidate the kinetic trends of emission enhancement for THIA in the presence of bacterial species.

assumes that (1) the fluorescence intensity is linearly proportional to the fluorophore concentration⁸⁹ and (2) the molar extinction coefficient (at the excitation wavelength) for the solution-free dye and for the cell-bound dye are the same (i.e., the perturbation of the absorption spectrum of THIA (Figure 2a) is due to the relatively slow processes producing the emission at 600 nm rather than to the initial dye–cell interaction ascribed to the enhancement at 480 nm).

Via the exponential terms of the mass-transport relation (eq 2), D and L determine the time constant of the fluorescence enhancement. These exponential terms, at the same time, do not depend on the dye concentration and depend on the cell count via q_n (eq 2) only indirectly.

To analyze the diffusion-driven kinetics (eqs 2 and 3) in a manner similar to that for the cell-induced emission enhancement, we fit the curves calculated from eq 3 to a monoexponential rise function ($n = 1$, eq 1a). The time constants, τ , obtained from the monoexponential fits, manifested a strong dependence on the sheet (i.e., cell–wall) thickness, L , and on the diffusion coefficient, D , rather than on the cell count (Figure 8).

For identical values of D and L , simulations of fluorescence enhancement using eqs 2 and 3 indeed revealed only about a 10% change in the time constant, τ , when the cell count was altered by 2 orders of magnitude (Figure 8). Concurrently, the time constant of fluorescence enhancement, τ , manifested a substantial dependence on the diffusion coefficient of the dye in the permeable media, D , and on the thickness of the permeable sheet, L (Figure 8). This model reveals the sensitivity of the staining kinetics to the type of species (via D and L) and to the type of staining agent (via D) rather than to their concentrations.

The diffusion-driven model of fluorescence enhancement (eqs 2 and 3) represented the observed lack of concentration dependence for the species-specific staining kinetics. This model, however, failed to provide a physically feasible quantification of the diffusivity of the stain. A diffusion coefficient of THIA on the order of $10^{-13} \text{ cm}^2 \text{ s}^{-1}$ was suggested for media with viscosity considerably

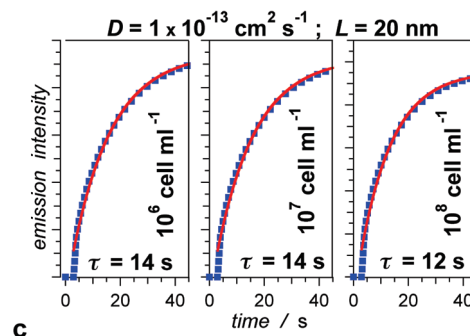
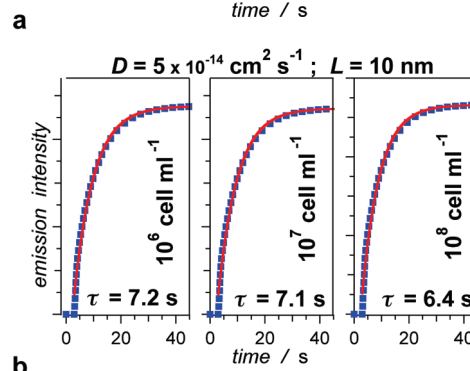
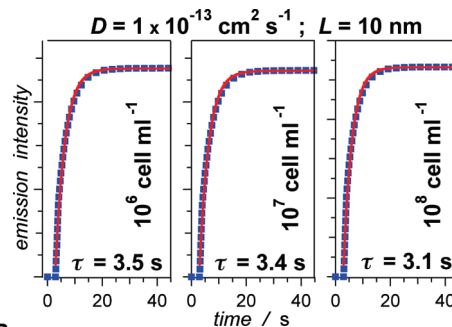


Figure 8. Simulated curves for fluorescence enhancement (eqs 2 and 3) resulting from the diffusion-driven migration of weakly fluorescent dye into the fluorogenic environment of the cell walls (Scheme 2). The blue squares represent the calculated values for different cell counts, different cell–wall thickness, L , and different diffusion coefficients, D . The solid red lines represent the corresponding monoexponential data fits ($n = 1$, eq 1a) that produced the different time constants, τ . For all calculations, $\Phi_C = 0.2$, $\Phi_W = 0.001$, $K = 2 \times 10^4$, $t_0 = 3 \text{ s}$, $V_C = 1 \text{ fl}$, $S_C = 6 \mu\text{m}^2$, and the number of exponential terms for the sum of (eq 2) was 10^3 .

exceeding the plausible viscosity of any material composing the bacterial cell wall. This finding implied the retention of the THIA migration, for example, as a result of binding processes.

A rough approximation of the characteristic diffusion time, τ_D , to an emission-enhancement time constant, τ , confirmed the unfeasibly small values of diffusion coefficients required to quantify the observed cell-staining kinetics. (The characteristic diffusion time depends on the characteristic diffusion length, l , and on the diffusion coefficient: $\tau_D = l_D^2/D$.⁹⁰) For the cell wall thickness, $l_D \approx L$, ranging between 10 and 100 nm, to ensure diffusion times as short as 1 s; for example, D had to range from 10^{-12} to $10^{-10} \text{ cm}^2 \text{ s}^{-1}$. For τ_D , compatible to the measured time constants on the order of 10 s, the values of D are even an order of magnitude smaller (i.e., 10^{-13} and $10^{-11} \text{ cm}^2 \text{ s}^{-1}$).

(89) Wan, J.; Thomas, M. S.; Guthrie, S.; Vullev, V. I. *Ann. Biomed. Eng.* **2009**, *37*, 1190–1205.

(90) Thomas, M. S.; Clift, J. M.; Millare, B.; Vullev, V. I. *Langmuir* **2010**, *26*, 2951–2957.

An important assumption for this diffusion-driven model was that the dye accumulated in the cell wall.⁵² Assuming that the THIA readily penetrated the intact cell membranes, a 1 μm diffusion length for the dye to migrate into the cell would require D to range from 10^{-8} to 10^{-9} $\text{cm}^2 \text{s}^{-1}$ for τ_D ranging from 1 to 10 s, respectively. These latter values of D still exceeded the reported diffusivities of ionic fluorophores in cytosol.^{91,92}

Representing the complex structure of bacterial cell walls of Gram-negative and Gram-positive species as a homogeneous gel-like sheet (Scheme 2) was indeed an oversimplification. Furthermore, such a two-state model (i.e., the dye is either in the cell or in the solution, eq 3) failed to account for aggregation processes that we ascribed as the potential reason for the observed perturbations of the shapes of the absorption and emission THIA spectra (Figure 2).

Nevertheless, such a model allowed for the demonstration of a negligible to nonexistent dependence of the staining kinetics on the cell count and on the dye concentration. Parameters L and D could be viewed as semiquantitative characteristics of the species and of their interactions with the staining agents representing effective thickness and effective diffusivity, respectively.

Conclusions

The kinetics of fluorescence staining of bacterium with 3,3'-diethylthiacyanine iodide manifested a lack of dependence on the dye concentration and on the cell count. An oversimplified model, based on diffusion-driven dye uptake, confirmed the lack of concentration dependence of the staining kinetics and was suggested for species and dye specificity. A surfactant additive, TWEEN 40, however, was required to obtain kinetic patterns that

were statistically different for the four different species that we studied. We believed that the lack of a statistically significant concentration dependence of species-specific and dye-specific staining kinetics has the potential to bring about a broad range of easily administrable bioanalytical assays beyond their Boolean nature.

Acknowledgment. This work was supported by the U.S. Department of Education, the National Science Foundation, and the U. C. Regents Faculty Development Award. We extend our gratitude to Profs. J. Schultz, V. Rodgers, and N. Schiller for helpful discussions on mass-transport models and bacterial physiology. The *E. coli* cells (TOP 10, Invitrogen) were donated by Prof. J. Liao.

Supporting Information Available: Experimental details: bacterial cultures and sample preparation,¹⁷ absorption and fluorescence measurements and imaging,^{93–100} and (3) data analysis,^{101,102} along with staining kinetic details for bacteria in the absence of surfactant additives. This material is available free of charge via the Internet at <http://pubs.acs.org>.

(93) Hu, J.; Xia, B.; Bao, D.; Ferreira, A.; Wan, J.; Jones, G.; Vullev, V. I. *J. Phys. Chem. A* **2009**, *113*, 3096–3107.

(94) Hong, C.; Bao, D.; Thomas, M. S.; Clift, J. M.; Vullev, V. I. *Langmuir* **2008**, *24*, 8439–8442.

(95) Wan, J.; Ferreira, A.; Xia, W.; Chow, C. H.; Takechi, K.; Kamat, P. V.; Jones, G.; Vullev, V. I. *J. Photochem. Photobiol., A* **2008**, *197*, 364–374.

(96) Jones, G., II; Yan, D.; Hu, J.; Wan, J.; Xia, B.; Vullev, V. I. *J. Phys. Chem. B* **2007**, *111*, 6921–6929.

(97) Mayers, B. T.; Vezenov, D. V.; Vullev, V. I.; Whitesides, G. M. *Anal. Chem.* **2005**, *77*, 1310–1316.

(98) Jones, G., II; Zhou, X.; Vullev, V. I. *Photochem. Photobiol. Sci.* **2003**, *2*, 1080–1087.

(99) Crosby, G. A.; Demas, J. N. *J. Phys. Chem.* **1971**, *75*, 991–1024.

(100) Nad, S.; Pal, H. *J. Phys. Chem. A* **2001**, *105*, 1097–1106.

(101) Bao, D.; Millare, B.; Xia, W.; Steyer, B. G.; Gerasimenko, A. A.; Ferreira, A.; Contreras, A.; Vullev, V. I. *J. Phys. Chem. A* **2009**, *113*, 1259–1267.

(102) Millare, B.; Thomas, M.; Ferreira, A.; Xu, H.; Holesinger, M.; Vullev, V. I. *Langmuir* **2008**, *24*, 13218–13224.

(91) Mastro, A. M.; Babich, M. A.; Taylor, W. D.; Keith, A. D. *Proc. Natl. Acad. Sci. U.S.A.* **1984**, *81*, 3414–3418.

(92) Swaminathan, R.; Bicknese, S.; Periasamy, N.; Verkman, A. S. *Biophys. J.* **1996**, *71*, 1140–1151.